



Lab on a Chip

Simultaneous quantification of blood rheology and oxygen saturation to evaluate affinity-modifying therapies in sickle cell disease

Journal:	<i>Lab on a Chip</i>
Manuscript ID	LC-ART-07-2022-000623.R1
Article Type:	Paper
Date Submitted by the Author:	17-Aug-2022
Complete List of Authors:	Hansen, Scott; University of Minnesota Twin Cities, Biomedical Engineering Wood, David; University of Minnesota Twin Cities, Biomedical Engineering

SCHOLARONE™
Manuscripts

Simultaneous quantification of blood rheology and oxygen saturation to evaluate affinity-modifying therapies in sickle cell disease

Scott Hansen¹ and David K. Wood^{1*}

¹Department of Biomedical Engineering, University of Minnesota, Minneapolis 55409 USA

*Correspondence: dkwood@umn.edu

Abstract

Sickle cell blood demonstrates oxygen-dependent flow behavior as a result of HbS polymerization during hypoxia, and these rheological changes provide a biophysical metric that can be used to quantify the pathological behavior of the blood. Relating these rheological changes directly to hemoglobin oxygen saturation would improve our understanding of SCD pathogenesis and the potential effects of therapeutic drugs. Towards this end, we have developed a microfluidic platform capable of spectrophotometric quantification of Hb-O₂ saturation and simultaneous evaluation of the accompanying rheological changes in SCD blood flow. We demonstrated the ability to measure changes in Hb-O₂ affinity and a restoration of oxygen-independent blood flow behavior after incubation with Voxelotor, an oxygen affinity modifying drug approved for use in SCD. We also identified regimes in Hb-O₂ saturation where the effects of HbS polymerization begin to take effect in contributing to pathological flow behavior, independent of Voxelotor treatment. In contrast, incubation with Voxelotor recovered oxygen-dependent blood flow over a range of P_{O₂}, providing a framework for understanding Voxelotor's therapeutic effect in lowering the P_{O₂} at which the requisite Hb-O₂ saturation is reached to observe pathological blood flow. These results help explain the mechanistic effects of Voxelotor and show the potential of this platform to identify affinity-modifying compounds and evaluate their therapeutic effect on blood flow.

Introduction

Sickle cell disease is an inherited blood disorder caused by a missense mutation at the 6th position of the β -globin subunit of hemoglobin, resulting in the substitution of a hydrophilic glutamic acid for a hydrophobic valine¹⁻³. Sickle hemoglobin polymerizes during deoxygenation, causing the cells to become rigid and lose their typical deformability⁴⁻¹⁰. The poorly deformable RBCs and elevation in blood viscosity can lead to vaso-occlusion in the microcirculation. Despite advances in treatment, average lifespans are still several decades shorter than the general population with devastating complications such as vaso-occlusive crisis (VOC), acute chest syndrome, stroke, and chronic organ failure¹¹⁻¹⁶. Oxygen affinity shifting small molecules such as BW12C¹⁷, Tucaresol¹⁸, Aes-103 (5HMF)¹⁹, and Voxelotor (GBT440)²⁰ have been investigated for their ability to indirectly inhibit HbS polymerization. Voxelotor is the only one to receive FDA approval after completion of the Phase III HOPE clinical trial (ClinicalTrials.gov Identifier: NCT03036813)²¹. However, there are concerns that shifting Hb-O₂ affinity may have unintended negative side-effects in this patient population where anemia is already severe²². The ideal drug candidate would directly act to inhibit HbS polymerization with little to no effect on oxygen transport, for which promising candidates now exist²³. Finding the degree to which affinity shifting drugs restore healthy blood flow behavior without impeding oxygen delivery remains an important goal in understanding their efficacy and safety.

In vitro model systems have proven to be useful tools in understanding the loss of sickle RBC deformability during deoxygenation and assessing the effects of drug therapies in SCD. Typically, measurement of RBC deformability and Hb-O₂ saturation requires separate measurements on multiple instruments. Such was the case for previous work using ektacytometry and spectroscopic methods to quantify the oxygen saturation corresponding to a loss of RBC deformability⁹. More recently, Voxelotor was found to enhance sickle RBC filterability and decrease the shear elastic modulus during micropipette aspiration of deoxygenated sickle RBCs²⁴. Separately, the potent affinity-modifying behavior of Voxelotor was quantified by collecting the oxygen equilibrium curves for treated samples using a Hemox analyzer²⁵. Combining Hb-O₂ measurement with biophysical analysis of SCD blood flow could reduce the number of assays and equipment required to evaluate affinity shifting molecules in sickle cell disease. Further, capturing changes in blood flow behavior under conditions mimicking the microcirculation reveals aspects of SCD blood rheology that may have more relevance *in vivo* than single cell assays. Microfluidic platforms modeled after the microcirculatory flow of the post-capillary

venules have previously been used to evaluate the oxygen-dependent nature of SCD blood rheology²⁶⁻²⁸. Combining spectrophotometric and blood rheology analyses on a single chip provides a method which can quantify Hb-O₂ saturation and the subsequent change in blood flow behavior. This method is particularly useful for identifying and evaluating oxygen affinity modifying compounds used to treat SCD from both a mechanistic and therapeutic perspective.

In this work, we describe a microfluidic platform for combined spectrophotometric determination of Hb-O₂ saturation and rheological assessment of SCD blood flow. This technology integrates multiple measurements onto a single microfluidic device, making direct measurements of SCD blood rheology in response to oxygen saturation possible. An important advancement is the implementation of two-wavelength spectrophotometric measurement of flowing blood under more physiologic microcirculatory flow conditions, rather than single RBCs or lysates. The optical absorption at each wavelength can be used to determine hemoglobin oxygen affinity empirically while simultaneously tracking blood flow using a particle image velocimetry algorithm on images acquired from high-speed cameras. To demonstrate the utility of this system, we used it to evaluate SCD blood samples that were incubated with Voxelator to quantify shifts in oxygen affinity and improvement in blood rheology. Voxelator's inhibitory action on HbS polymerization was marked by a reduced degree of hyperviscous blood flow during deoxygenation. Voxelator serves as a model affinity-shifting drug in this study, and our results may serve as a useful benchmark in weighing the benefits of preventing HbS polymerization against the potentially harmful effects of increasing Hb-O₂ affinity among other therapeutic candidates. The ability to quantify Hb-O₂ saturation and relate it directly to SCD blood rheological behavior provides a powerful tool in understanding potential drug treatments from a mechanistic perspective and their potential for therapeutic impact.

Methods

Sample Collection

This study was conducted under protocol STUDY0003, which was approved by the Institutional Review Boards at Children's Hospital and Clinics of Minnesota, the University of Minnesota Medical Center, and the University of Minnesota. Informed consent was obtained from all subjects prior to participation in this study and prior to any blood or data collection. Samples from volunteers were collected into citrate or EDTA tubes and stored for no more than 48 hours at 4°C before analysis to minimize 2,3 diphosphoglycerate (2,3 DPG) degradation^{29,30}. Blood samples from 11 individuals were used in this study, including four of genotype HbAA, five of genotype HbSS, one of genotype HbSC, and one of genotype HbS/B⁺ thalassemia. Complete blood counts and hemoglobin variant analysis is shown in Table S1. Data for some values was not measured.

Whole blood samples were centrifuged twice at 400g for 5 minutes and washed with HS-500 Hemox buffer solution (TCS Scientific Corp., New Hope, PA) to remove the native plasma. Packed red blood cells were taken from the pellet following a final centrifugation at 400g for 10 minutes and resuspended in Hemox buffer to reach a final hematocrit of ~25%. Dimethyl sulfoxide (DMSO) at a concentration of 0.5% v/v percent or 500µmol/L Voxelotor (Global Blood Therapeutics, South San Francisco, CA) dissolved in DMSO were added to the vehicle control and treated samples respectively. All sample volumes were stirred at 100rpm while incubating at 37°C for one hour prior to being perfused through the microfluidic device.

Microfluidic Platform

Modifications were made to a previously reported microfluidic device to allow for spectrophotometric analysis^{27,31}. Unique to this device is a gap in the hydration layer that serves as a viewing window for the blood channel (Figure 1B, inset). This viewing window maintains a constant incident light intensity on the device by preventing air bubbles in the hydration layer from obscuring the imaging region of interest. The device consists of three polydimethylsiloxane (PDMS) layers separated by 100µm PDMS membranes fabricated using standard photolithography and replication techniques²⁷ (Figure 1A). The bottom blood layer is bonded directly to the glass slide and has a single bifurcation that diverts flow to two 15µm x 15µm square channels—a bypass channel and an observation channel. Overlaid on top of the blood layer is a hydration layer with 100µm tall channels to prevent dehydration of the sample.

Syringe pumps (NE-500, New Era Pump Systems) perfuse Dulbecco's phosphate buffered saline (DPBS) through two independent hydration channels overlaying the bypass and observation channels of the blood layer at a rate of 500ul/h. The top gas layer is 4-5mm thick with 150 μ m features covering the bypass and observation regions for independent oxygen control of each channel. The P_{O_2} supplied to the observation channel is cycled between atmospheric and hypoxic oxygen levels in 10mmHg increments using a previously described gas mixing system²⁸ (Figure 2C, i). On-chip oxygen levels are confirmed using a fiber optic oxygen sensor ((NeoFox-GT, Ocean Optics, Dunedin, FL) connected to the gas outlet of the observation channel. A compressed air cylinder (21% O_2 , 74% N_2 , 5% CO_2) supplies the bypass channel with a constant supply of air for the duration of the experiment.

Image Acquisition

Devices were mounted on a Zeiss Axio Vert.A1 microscope (Carl Zeiss, Oberkochen, Germany) in a 37°C temperature-controlled environment. Each device was primed with 2% bovine serum albumin (BSA) in DPBS to passivate the PDMS channel walls and prevent red cell adhesion. The prepared samples were then added to the device under the control of a pressure regulator to achieve a steady-state initial velocity of 300 μ m/s and a transit time of ~33 seconds through the channel. The driving pressure was held constant for the duration of the experiment to isolate oxygen-dependent flow behavior (PCD-15PSIG, Alicat Scientific).

Images of the observation channel are captured within the viewing window using a 40x objective and the condenser diaphragm open 50% to enhance contrast. Figure 1C shows the microscope setup and the light path from the white LED light source. The light transmitted through the channel is diverted to two high-speed cameras by a 50/50 beam splitter after passing through the specimen (GS3-U3-23S6M-C, FLIR, Wilsonville, OR). The cameras are triggered sequentially to capture 4-frame bursts of images at each wavelength of interest. The frame-to-frame feature displacements are tracked in real time using the Kanade-Lucas-Tomasi (KLT) tracking algorithm in Matlab (Mathworks, Natick, MA). The blood velocity through the channel is determined based on the calculated displacement and time stamp of each frame.

For Hb- O_2 determination, a method developed by di Caprio et al., for single cell analysis of oxygen saturation was used for resuspended whole blood samples³². Figure 2A provides a schematic illustration of the theoretical framework behind the oxygen saturation measurements. Each high-speed camera is fitted

with a 10nm bandpass optical filter with center wavelengths of 555nm and 575nm (Omega Optical, Battleboro, VT) corresponding to local peaks in the molar extinction coefficients of Hb and Hb-O₂ respectively (Figure 2B) ³³. During periods of hypoxia, the transmitted light intensity is minimized at 555nm and maximized at 575nm due to the relatively high molar extinction coefficient of Hb-O₂ at 575nm compared to 555nm (Figure 2C, ii). The absorbance is calculated from the output intensities at each wavelength and used to determine the Hb-O₂ saturation (Figure 2C, iii). The advantage of using resuspended whole blood over using lysates as in traditional spectrophotometry is that rheological changes in blood flow can be observed concurrently with Hb-O₂ dissociation. In SCD, HbS polymerization during periods of hypoxia causes RBCs to become rigid and the blood becomes hyper-viscous, obstructing blood flow as a result. This increase in apparent viscosity increases the resistance to flow in the channel and decreases the flow rate, which can be detected as a change in blood velocity with the velocimetry method described earlier. An oxygen cycling protocol was used to observe these fluctuations in blood flow behavior that are dependent on Hb-O₂ saturation (Figure 2C, iv). With this platform, changes in Hb-O₂ saturation and rheological behavior as a result of hypoxia can be quantified.

Statistical Analysis

Sample responses for each patient sample were evaluated pairwise between treated and untreated groups using a one- or two-tailed Wilcoxon signed-rank test where indicated. Where multiple comparisons were made, a non-parametric Friedman test with Dunn's correction was used to determine statistical significance. Correlations are reported as the Spearman correlation coefficient. All statistical tests were performed with a significance level of $\alpha=0.05$.

Results

Quantifying Oxygen Affinity Under Bulk Blood Flow

The relative abundance of Hb and Hb-O₂ can be determined using a spectrophotometric method due to their unique optical absorption profiles in the green-yellow region of the visible light spectrum. The physical changes in optical absorption under varying P_{O₂} is manifested as differences in the transmitted light intensity at 555nm and 575nm. We used the equations developed by Di Caprio et al., for the optical determination of Hb-O₂ saturation³². The transmitted light intensity (I) at each wavelength is recorded as the average channel intensity of the flowing red blood cells during the oxygen cycling protocol described above (Figure 2C, ii). Figure 3A (top) shows the RBCs under flow with the dashed lines indicating the region of interest where the pixel values are averaged to determine the transmitted light intensity. The recorded intensity values were then converted into instantaneous absorbances (A) for the duration of the experiment using Equation 1, which accounts for the maximum and minimum observable pixel intensity.

$$A = -\ln\left(\frac{I - I_{ref,dark}}{I_0 - I_{ref,dark}}\right) \quad (1)$$

The incident light intensity (I₀) is determined prior to each experiment as the average recorded intensity in the channel after BSA has been introduced, prior to the addition of the blood sample (Figure 3A, middle). The contribution of ambient light is subtracting from the incident and transmitted light intensity by determining the dark reference intensity (I_{ref,dark}) when the microscope light source is turned completely off (Figure 3A, bottom). Given the normalized absorption (A), the area of the region of interest (pa), and the molecular weight of Hb (MW_{Hb}), the extinction at each wavelength can be determined using Equation 2.

$$E_{555/575} = A_{555/575} \cdot pa \cdot MW_{Hb} \quad (2)$$

The empirically derived extinction output relies on contributions from the absorption of both Hb and Hb-O₂. Equations 3 and 4 factor in these contributions as a sum of the extinctions of both Hb and Hb-O₂ at each wavelength. The tabulated molar extinction coefficients account for the presence of Hb and Hb-O₂ and in determining the abundance (mass) of Hb and Hb-O₂³³. Solving

these equations simultaneously yields mass values for oxygenated Hb (M_o) and deoxygenated Hb (M_d).

$$E_{555} = e_{555}^o M_o + e_{555}^d M_d \quad (3)$$

$$E_{575} = e_{575}^o M_o + e_{575}^d M_d \quad (4)$$

Figure 3B shows the resulting Hb-O₂ saturation values, defined as $S = M_o / (M_o + M_d)$, for each P_{O₂} in the experimental protocol (See Figure 2C, i). The derived saturation values do not fall between 0% at 0mmHg O₂ and 100% at 160mmHg O₂, but within a range of oxygen-dependent intermediate values. This was not entirely unexpected as this result was seen in similar work³². Thus, we established a normalization scheme to correct the upper and lower bounds to reflect 100% saturation at 160mmHg O₂ and 0% saturation at 0mmHg O₂ P_{O₂} on the device (See Figure S1). The dashed red lines in Figure 3B show the median saturation for all 160mmHg O₂ cycles and the saturation at 0mmHg O₂. The magnitude of this difference was assumed to be the maximum change in signal corresponding to complete desaturation for each sample. Therefore, the magnitude of the signal change in the untreated condition for each sample was used for normalizing both the untreated and treated sample data. This was done to account for the fact that Voxelator may prevent complete Hb-O₂ desaturation and would therefore not have a suitable lower limit for normalization.

The oxygen affinity (p50) of each untreated sample was determined by fitting a Hill equation of the form found in Equation 5. A second order polynomial provided a better fit of the data from the treated case since those samples did not necessarily reach complete desaturation. The Hill equation was the best fit for the untreated condition, though a second order polynomial fitting did not significantly change the result (Table S2). Figure 3C shows the reconstructed oxygen equilibrium curves (OEC) with and without Voxelator for a single sample based on the P_{O₂} recorded by the fiber optic oxygen sensor at the gas channel outlet of the device.

$$S = \frac{(P/P_{50})^n}{1 + (P/P_{50})^n} \quad (5)$$

Figure 3D shows the oxygen equilibrium curves based on the fitted data for all samples with and without Voxelotor. After incubation with Voxelotor, samples had a left-shifted OEC, indicating an increased oxygen affinity, as expected. Figure 3E shows the statistically significant pairwise analysis of the p50 values for each patient sample before and after treatment (One-tailed, Wilcoxon Signed rank test, $\alpha = 0.05$). The mean p50 was decreased by 10.42mmHg, which agrees with previously reported values based on the same concentration of Voxelotor.

Increased Viscosity of SCD Blood During Hypoxia is Dependent on Hb-O₂ Saturation

During hypoxia, hydrophobic residues on the HbS tetramer interact to form rigid polymer fiber, increasing the viscosity of the blood and altering SCD blood flow behavior^{6,34}. In a microfluidic device, this increase in viscosity can be observed as a change in the tracked velocity of the blood through the channel²⁶. Figure 4A shows a representative image of the blood as it flows through the channel (4A, top) and the tracked feature displacements between video frames used to monitor the velocity of the blood (4A, bottom). During the transition from atmospheric O₂ levels to hypoxia, the velocity of blood flow is substantially reduced. We calculated the area under the mean velocity response curve (Figure 4B) as a metric for quantifying the sensitivity of the blood sample rheological behavior to hypoxia. We compared the untreated vehicle control condition versus the Voxelotor treated condition and found that there was a significant decrease in AUC (p-value = 0.0078), representing a shift toward oxygen-independent flow behavior (Figure 4C). As an overall metric of pathological rheological behavior, the reduction in AUC indicates that Voxelotor has a beneficial effect in restoring healthy blood flow.

Rheological changes corresponding to specific levels of Hb-O₂ saturation can also be directly observed. In Figures 4D-G, we quantify the blood flow response using two different metrics: P_{O₂} and Hb-O₂ saturation. Figure D shows the mean velocity drop during hypoxia of SCD blood samples before and after treatment with 500uM Voxelotor. We observed a consistent recovery of

oxygen-independent flow behavior at each P_{O_2} of $\sim 15\%$ between the two groups. We defined a criterion to quantify a velocity response threshold as the interpolated P_{O_2} where the mean velocity changed less than 3% of the velocity of the fully oxygenated condition. There was a small, but statistically significant reduction of 4.93% in the P_{O_2} where the threshold criterion was met among the treated samples. Due to the dependence of polymerization on Hb- O_2 saturation and not necessarily P_{O_2} , we performed the same analysis using the measured saturation values in Figures 4F-G. Above 40% saturation, there was little difference in the velocity response of the untreated and treated samples. Below 40% saturation, the difference in the velocity response was $\sim 10\text{-}15\%$ between the treated and untreated samples. The large difference at lower Hb- O_2 could be a result of the smaller sample size of the treated group ($n=6$) and the untreated group ($n=16$). Voxelotor prevented some of the samples from reaching the lowest threshold levels of saturation and those were not represented in the analysis. At physiologically relevant Hb- O_2 saturation, the velocity response was dependent on saturation regardless of the treatment condition. Using the same threshold criterion as before, we observed that the onset of oxygen-dependent flow before did not occur until the Hb- O_2 saturation reached $\sim 75\%$ ($\sigma_{\text{Untreated}} = 76.6\%$, $\sigma_{\text{Treated}} = 75.5\%$).

Transient Effects of Voxelotor on Pathological Blood Flow

We quantified the rates of Hb- O_2 desaturation and blood flow deceleration to uncover Voxelotor's role in slowing Hb- O_2 dissociation and the resulting biophysical effects of blood flow. Figure 5A shows the normalized Hb- O_2 saturation (blue) and blood velocity (orange) in response to a sudden decrease in oxygen tension (black). The velocity and saturation responses were segmented into regions based on the largest mean signal changes after introducing hypoxic conditions to the device. The data from each segment was fitted to a first order polynomial to determine the maximum slope of the signal, taken as the rates of desaturation and deceleration (Figure 2B). Figure 5C shows the desaturation rates for the untreated and treated conditions. The rate of desaturation decreased significantly with increasing P_{O_2} on the device (Kruskal-Wallis test, $p\text{-value} = <0.0001$). Additionally, the desaturation rate was lower when the samples had been incubated with Voxelotor, indicating an inhibitory effect on Hb- O_2 dissociation. Similarly, the rate of deceleration also decreased significantly with increasing P_{O_2} on the device (Figure 5F) (Kruskal-Wallis test, $p\text{-value} = <0.0001$), and the rate of deceleration was slower among the samples treated with Voxelotor compared to the untreated control condition. We analyzed the

untreated samples and found that Hb-O₂ dissociation and blood flow deceleration were both correlated with oxygen affinity at low oxygen tensions where the responses to hypoxia for both parameters were large (Figures 5D and 5F).

Discussion

The finding in this study that Voxelotor restores oxygen-independent blood rheology agrees with previous work by Dufu et al., which demonstrated improved filterability, lower membrane shear elastic modulus, and lower whole blood viscosity in samples treated with Voxelotor. The platform presented here allows for the observation of these effects on a single device under more physiologically relevant conditions while simultaneously capturing the degree of Hb-O₂ saturation under which these changes take place. For a given P_{O₂}, Voxelotor decreased the steady state velocity response among the samples up to 15-35% and slowed the rate of onset for these changes to occur. This slower, weaker response could allow cells to pass through the microcirculation before significant HbS polymerization occurs, decreasing the likelihood of vaso-occlusion in tissues of a given P_{O₂} and preventing cell damage from cyclic HbS polymerization. Further, the average onset of impairment after ~25% desaturation may help explain why hypoxic organs like the kidney are prone to chronic organ damage even while most RBCs are able to pass through the microcirculation⁴⁴⁻⁴⁷.

Even under complete hypoxia, Voxelotor had a beneficial effect in reducing the degree of hyperviscosity, an observation also observed using cone/plate viscometry using whole blood samples. This effect in the device presented here can be explained by incomplete Hb-O₂ dissociation of the treated samples during their transit through the microfluidic channel. Given an estimated 35% drug binding to Hb, it is possible that there remains a population of bound R-state Hb even after the system reaches steady state hypoxia. To account for the apparent incomplete Hb-O₂ dissociation, we assumed that the untreated blood reached 100% Hb-O₂ saturation at 160mmHg P_{O₂} and 0% saturation at P_{O₂}. Previous work using this device shows this to be a reasonable assumption based on O₂ diffusion modeling and experimental confirmation using an oxygen sensitive dye²⁷. Treated samples were normalized against the raw maximum and minimum saturation values from the untreated control condition as shown in Figure S1. This correction yielded a shift in p50 that was consistent with previous findings and highlights the large effect of Voxelotor on Hb-O₂ oxygen affinity. Using this calibration, the degree of

rheological impairment was driven by Hb-O₂ saturation and appeared independent of oxygen affinity. In the range of physiological oxygen saturation above 40%, the rheology responses were nearly identical for treated and untreated samples. At 40% saturation and below however, we observed that the treated sample responses were smaller than for untreated samples. This may be explained in part by the small number of samples in the treated group that reached extremely low levels of Hb-O₂ saturation, which were also biased toward samples with weaker responses.

The benefits to blood rheology must be weighed against the potential risks associated with impaired oxygen delivery to the tissues as noted by Hebbel and Hedlund²². They prescribe a cautious approach to implementing affinity-modifying drugs in patients with sickle cell disease. The microfluidic device described here can serve as a preliminary risk-benefit analysis of affinity-modifying compounds. Our results provide a baseline for assessing the risks and efficacy of other affinity-modifying drugs against Voxelotor, which is the only drug of its kind to have received FDA approval. Compounds that restore healthy rheological behavior with little effect on oxygen affinity would be preferable to those that show similar rheological benefits, but with very high Hb-O₂ affinity modification. Ideally, a drug could be found that directly inhibits HbS polymerization without the potential risks associated with reduced oxygen delivery. Recently, VZHE-039 has been shown to have a substantial inhibitory effect on sickling with evidence suggesting that oxygen-independent mechanisms are directly inhibiting HbS polymerization²³. The approach presented in this work may be useful in evaluating the potential risks and benefits of affinity-modifying compounds, providing a pre-clinical screening tool for this class of drugs. Notably, the response to voxelotor in our steady state rheology measurement is relatively small compared to single cell measurements,^{24,25,35,36} which is likely due to the complex contribution of single cell properties to overall viscosity. Nonetheless, the change in signal is robust and easily measurable with our platform's sensitivity. Additionally, a combinatorial approach such as this reduces the need for multiple measurements, further accelerating *in vitro* drug evaluation. In this work, rheological and spectroscopic measurement of SCD blood were successfully combined on a single microfluidic device, providing a method to accelerate evaluation of prospective drug candidates for this devastating disease.

Acknowledgments

We thank the patients at Children's Hospital and Clinics of Minnesota for their generous blood donations and the sickle care team, including Dr. Steve Nelson, Ashley Kinsella, Pauline Mitby, Ali Koste, Rachel Hinsch, and Emily Olson for blood sample collection. We thank Ethan Schonbrun for useful conversations about the spectrophotometric method. We acknowledge funding from the National Heart, Lung, and Blood Institute under grant R01HL132906. Portions of this work were conducted in the Minnesota Nano Center, which is supported by the National Science Foundation through the National Nanotechnology Coordinated Infrastructure (NNCI) under Award Number ECCS-2025124.

Conflicts of Interest

The authors have no conflicts to declare.

Author Contributions

Conceptualization: SH, DKW

Methodology: SH

Investigation: SH

Visualization: SH

Supervision: DKW

Writing—original draft: SH

Writing—review & editing: DKW

References

- 1 Ingram, V. M. Gene mutations in human haemoglobin: the chemical difference between normal and sickle cell haemoglobin. *Nature* **180**, 326-328 (1957). <https://doi.org:10.1038/180326a0>
- 2 Ingram, V. M. Abnormal human haemoglobins. III. The chemical difference between normal and sickle cell haemoglobins. *Biochim Biophys Acta* **36**, 402-411 (1959). [https://doi.org:10.1016/0006-3002\(59\)90183-0](https://doi.org:10.1016/0006-3002(59)90183-0)
- 3 Frenette, P. S. & Atweh, G. F. Sickle cell disease: old discoveries, new concepts, and future promise. *J Clin Invest* **117**, 850-858 (2007). <https://doi.org:10.1172/JCI30920>
- 4 Pauling, L., Itano, H. A. & et al. Sickle cell anemia a molecular disease. *Science* **110**, 543-548 (1949). <https://doi.org:10.1126/science.110.2865.543>
- 5 Bunn, H. F. Pathogenesis and treatment of sickle cell disease. *N Engl J Med* **337**, 762-769 (1997). <https://doi.org:10.1056/NEJM199709113371107>
- 6 Eaton, W. A. & Hofrichter, J. Sickle cell hemoglobin polymerization. *Adv Protein Chem* **40**, 63-279 (1990). [https://doi.org:10.1016/s0065-3233\(08\)60287-9](https://doi.org:10.1016/s0065-3233(08)60287-9)
- 7 Ferrone, F. A., Hofrichter, J. & Eaton, W. A. Kinetics of sickle hemoglobin polymerization. II. A double nucleation mechanism. *J Mol Biol* **183**, 611-631 (1985).
- 8 Klug, P. P., Lessin, L. S. & Radice, P. Rheological aspects of sickle cell disease. *Arch Intern Med* **133**, 577-590 (1974).
- 9 Sorette, M. P., Lavenant, M. G. & Clark, M. R. Ektacytometric measurement of sickle cell deformability as a continuous function of oxygen tension. *Blood* **69**, 316-323 (1987).
- 10 Ballas, S. K. & Mohandas, N. Sickle red cell microrheology and sickle blood rheology. *Microcirculation* **11**, 209-225 (2004). <https://doi.org:10.1080/10739680490279410>
- 11 Kato, G. J. *et al.* Sickle cell disease. *Nat Rev Dis Primers* **4**, 18010 (2018). <https://doi.org:10.1038/nrdp.2018.10>
- 12 Stuart, M. J. & Nagel, R. L. Sickle-cell disease. *Lancet* **364**, 1343-1360 (2004). [https://doi.org:10.1016/S0140-6736\(04\)17192-4](https://doi.org:10.1016/S0140-6736(04)17192-4)
- 13 Chaturvedi, S. & DeBaun, M. R. Evolution of sickle cell disease from a life-threatening disease of children to a chronic disease of adults: The last 40 years. *Am J Hematol* **91**, 5-14 (2016). <https://doi.org:10.1002/ajh.24235>
- 14 Platt, O. S. *et al.* Mortality in Sickle-Cell Disease - Life Expectancy and Risk-Factors for Early Death. *New Engl J Med* **330**, 1639-1644 (1994). <https://doi.org:10.1056/Nejm199406093302303>
- 15 Powars, D. R., Chan, L. S., Hiti, A., Ramicone, E. & Johnson, C. Outcome of sickle cell anemia: a 4-decade observational study of 1056 patients. *Medicine (Baltimore)* **84**, 363-376 (2005). <https://doi.org:10.1097/01.md.0000189089.45003.52>
- 16 Quinn, C. T. Sickle cell disease in childhood: from newborn screening through transition to adult medical care. *Pediatr Clin North Am* **60**, 1363-1381 (2013). <https://doi.org:10.1016/j.pcl.2013.09.006>
- 17 Beddell, C. R. *et al.* Substituted benzaldehydes designed to increase the oxygen affinity of human haemoglobin and inhibit the sickling of sickle erythrocytes. *Br J Pharmacol* **82**, 397-407 (1984). <https://doi.org:10.1111/j.1476-5381.1984.tb10775.x>

- 18 Arya, R., Rolan, P. E., Wootton, R., Posner, J. & Bellingham, A. J. Tucarezol increases oxygen affinity and reduces haemolysis in subjects with sickle cell anaemia. *Br J Haematol* **93**, 817-821 (1996). <https://doi.org:10.1046/j.1365-2141.1996.d01-1744.x>
- 19 Abdulmalik, O. *et al.* 5-hydroxymethyl-2-furfural modifies intracellular sickle haemoglobin and inhibits sickling of red blood cells. *Brit J Haematol* **128**, 552-561 (2005). <https://doi.org:10.1111/j.1365-2141.2004.05332.x>
- 20 Lehrer-Graiwer, J. *et al.* GBT440, a Potent Anti-Sickling Hemoglobin Modifier Reduces Hemolysis, Improves Anemia and Nearly Eliminates Sickle Cells in Peripheral Blood of Patients with Sickle Cell Disease. *Blood* **126** (2015).
- 21 Vichinsky, E. *et al.* A Phase 3 Randomized Trial of Voxelotor in Sickle Cell Disease. *N Engl J Med* **381**, 509-519 (2019). <https://doi.org:10.1056/NEJMoa1903212>
- 22 Hebbel, R. P. & Hedlund, B. E. Sickle hemoglobin oxygen affinity-shifting strategies have unequal cerebrovascular risks. *Am J Hematol* **93**, 321-325 (2018). <https://doi.org:10.1002/ajh.24975>
- 23 Abdulmalik, O. *et al.* VZHE-039, a novel antisickling agent that prevents erythrocyte sickling under both hypoxic and anoxic conditions. *Sci Rep* **10**, 20277 (2020). <https://doi.org:10.1038/s41598-020-77171-2>
- 24 Dufu, K., Patel, M., Oksenberg, D. & Cabrales, P. GBT440 improves red blood cell deformability and reduces viscosity of sickle cell blood under deoxygenated conditions. *Clin Hemorheol Microcirc* **70**, 95-105 (2018). <https://doi.org:10.3233/CH-170340>
- 25 Oksenberg, D. *et al.* GBT440 increases haemoglobin oxygen affinity, reduces sickling and prolongs RBC half-life in a murine model of sickle cell disease. *Br J Haematol* **175**, 141-153 (2016). <https://doi.org:10.1111/bjh.14214>
- 26 Wood, D. K., Soriano, A., Mahadevan, L., Higgins, J. M. & Bhatia, S. N. A Biophysical Indicator of Vaso-occlusive Risk in Sickle Cell Disease. *Sci Transl Med* **4** (2012). <https://doi.org:ARTN123ra26>
- 10.1126/scitranslmed.3002738
- 27 Valdez, J. M., Datta, Y. H., Higgins, J. M. & Wood, D. K. A microfluidic platform for simultaneous quantification of oxygen-dependent viscosity and shear thinning in sickle cell blood. *APL Bioeng* **3**, 046102 (2019). <https://doi.org:10.1063/1.5118212>
- 28 Lu, X. R., Wood, D. K. & Higgins, J. M. Deoxygenation Reduces Sickle Cell Blood Flow at Arterial Oxygen Tension. *Biophys J* **110**, 2751-2758 (2016). <https://doi.org:10.1016/j.bpj.2016.04.050>
- 29 Bennett-Guerrero, E. *et al.* Evolution of adverse changes in stored RBCs. *Proc Natl Acad Sci U S A* **104**, 17063-17068 (2007). <https://doi.org:10.1073/pnas.0708160104>
- 30 Yoshida, T., Prudent, M. & D'Alessandro, A. Red blood cell storage lesion: causes and potential clinical consequences. *Blood Transfus* **17**, 27-52 (2019). <https://doi.org:10.2450/2019.0217-18>
- 31 Hansen, S., Wood, D. K. & Higgins, J. M. 5-(Hydroxymethyl)furfural restores low-oxygen rheology of sickle trait blood in vitro. *Br J Haematol* **188**, 985-993 (2020). <https://doi.org:10.1111/bjh.16251>
- 32 Di Caprio, G., Stokes, C., Higgins, J. M. & Schonbrun, E. Single-cell measurement of red blood cell oxygen affinity. *Proc Natl Acad Sci U S A* **112**, 9984-9989 (2015). <https://doi.org:10.1073/pnas.1509252112>

- 33 Prah, S. *Tabulated molar extinction coefficient for hemoglobin in water.*, <<http://omlc.org.edu/spectra/hemoglobin/summary.html>> (1998).
- 34 Barabino, G. A., Platt, M. O. & Kaul, D. K. Sick cell biomechanics. *Annu Rev Biomed Eng* **12**, 345-367 (2010). <https://doi.org:10.1146/annurev-bioeng-070909-105339>
- 35 Dufu, K. & Oksenberg, D. GBT440 reverses sickling of sickled red blood cells under hypoxic conditions in vitro. *Hematol Rep* **10**, 7419 (2018). <https://doi.org:10.4081/hr.2018.7419>
- 36 Boisson, C. *et al.* Effects of Genotypes and Treatment on Oxygenscan Parameters in Sick Cell Disease. *Cells* **10** (2021). <https://doi.org:10.3390/cells10040811>

Figure 1

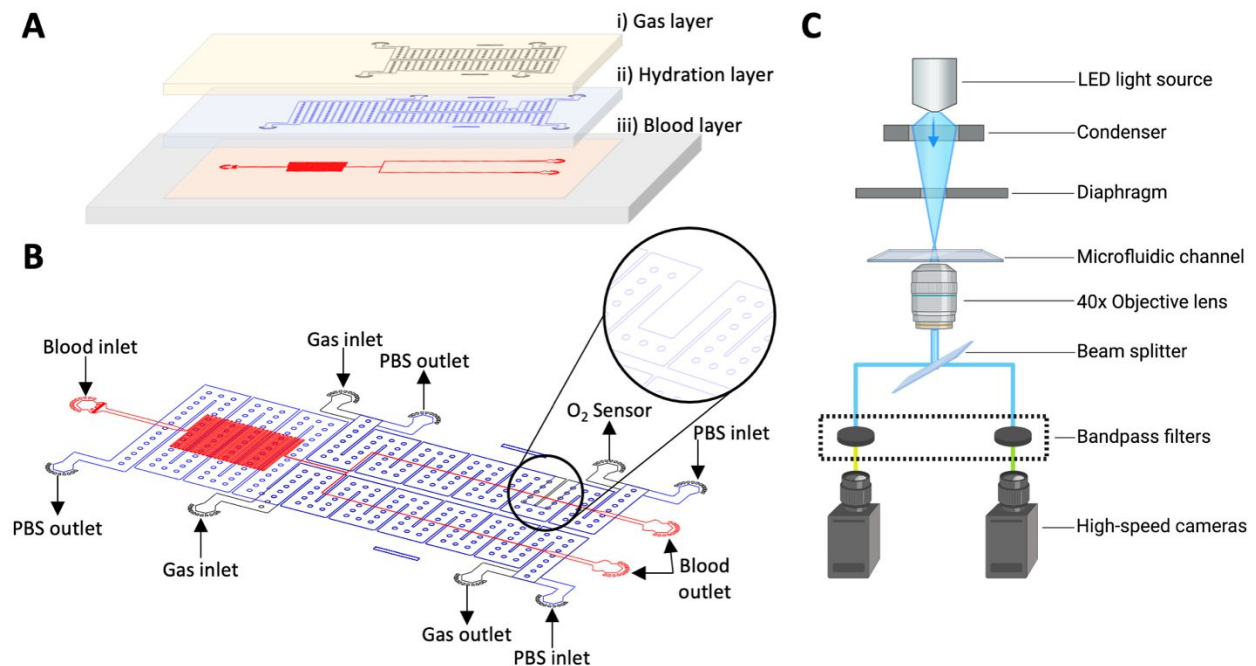


Figure 1 Microfluidic platform schematic. (A) Three-layer PDMS device consists of a top gas layer, a middle hydration layer, and a bottom blood layer bonded to a glass slide. (B) Blood is perfused from the inlet to the outlet reservoir of the blood layer (red) at a constant pressure. Syringe pumps at the hydration layer (blue) inlets flow PBS through the device at 500 μ L/hr. Mixed gas is supplied to the experimental side of the gas layer (black) and recorded by a fiberoptic oxygen sensor. The gas supplied to the bypass channel is 160mmHg O₂. (C) Light from a white LED light source passes through the sample and is diverted to two high-speed cameras. Each camera is fitted with either a 555nm or 575nm CWL, 10nm bandpass filter. Adapted from “Transmission Electron Microscopy (TEM)”, by BioRender.com (2020). Retrieved from <https://app.biorender.com/biorender-templates>.

Figure 2

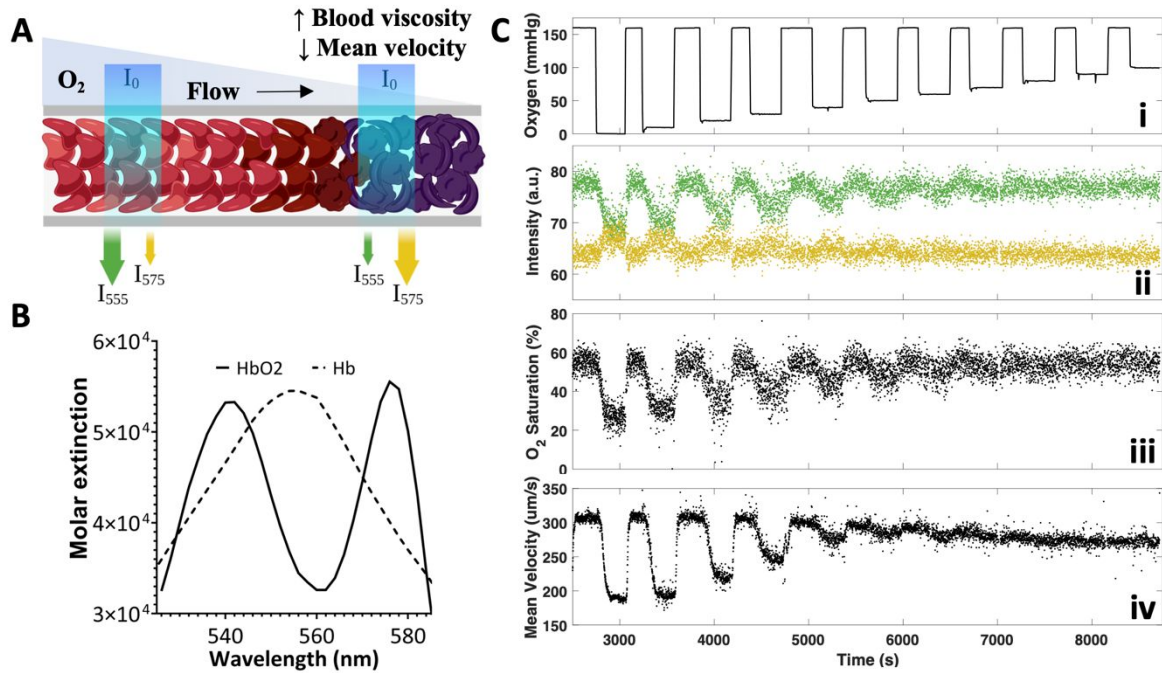


Figure 2 Simultaneous recording of Hb-oxygen saturation and blood flow behavior is possible through the unique absorption spectra of oxyHb and deoxyHb. (A) Schematic representation of the optical absorbance at the wavelengths of interest under different oxygen conditions. At 160mmHg O_2 , the absorption of oxyHb approaches a local minimum at 555nm. Conversely, under hypoxia, the absorption of oxyHb reaches a local maximum at 575nm and vice versa for deoxyHb. It follows that the output intensity for oxyHb is maximized at 555nm and minimized at 575nm and vice versa for deoxyHb. Created with Biorender.com. (B) Molar extinction coefficients of oxyHb (solid) and deoxyHb (dashed) reproduced from tabulated values made available by S. Praul³⁶. (C) Representative experimental data from oxygen cycling protocol with increasing P_{O_2} during hypoxia in 10mmHg increments (i). Intensity output at 555nm (green) and 575nm (yellow) during oxygen cycling (ii). Derived O_2 saturation using the intensity outputs at each wavelength to solve Equations 1-3 (iii). Mean tracked velocity of blood in the channel using Lucas-Kanade-Tomasi (LKT) feature tracking in Matlab (iv).

Figure 3

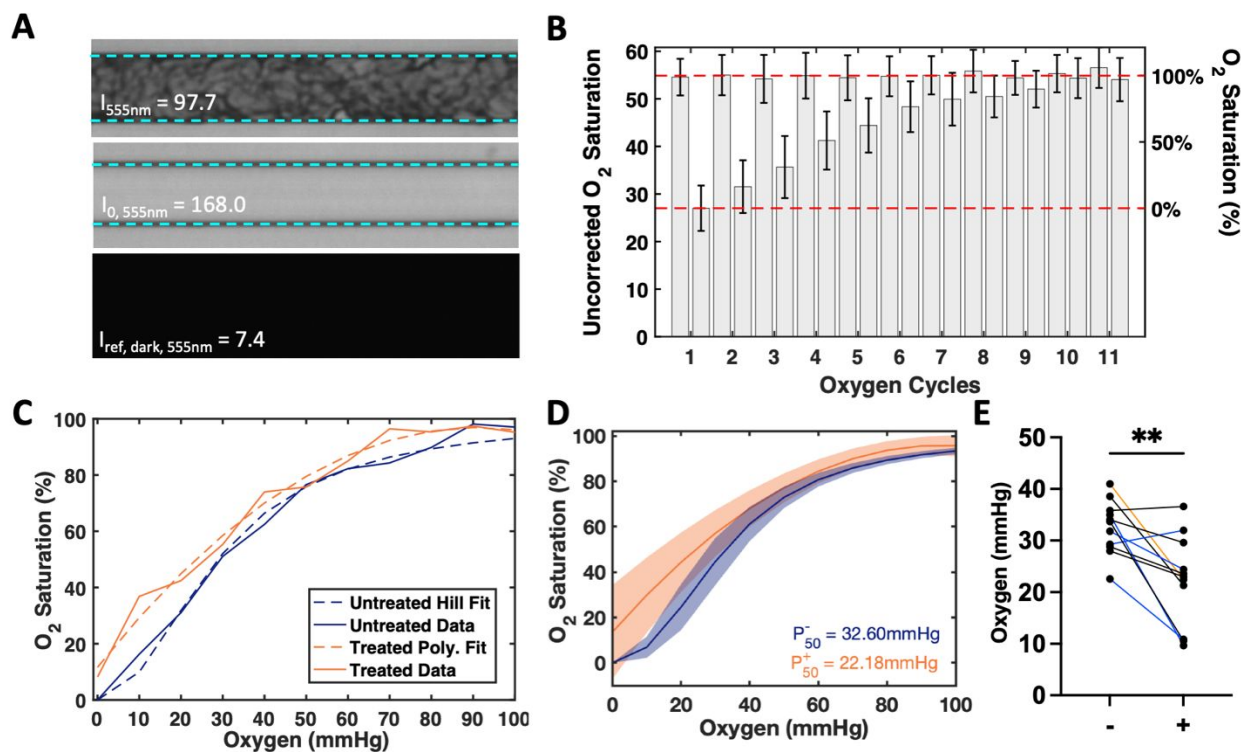


Figure 3 Quantification of Hb-O₂ saturation under bulk flow conditions in the presence or absence of an affinity-modifying small molecule, GBT-440 (Voxelator). (A) Reference intensities used in Equation 1 for the transmitted light intensity (top), the incident light intensity (middle), and the dark reference intensity (bottom). (B) Mean saturation output from the mass outputs using Equations 3 and 4. Red dashed lines represent the bounds of normalization as the median saturation at 160mmHg and 0mmHg O₂. The upper and lower bounds of the untreated sample are used for normalizing both the untreated and treated condition assuming that Voxelotor-treated samples may not reach complete O₂ desaturation. (S.Figure 1) (C) Normalized oxygen saturation values before (blue, solid) and after (orange, solid) incubation with 500uM Voxelotor. The dashed line represents the curve fit using the Hill equation and a second-order polynomial for the untreated and treated conditions, respectively. (D) Samples exhibited a left-shifted O₂ saturation curve after incubation with Voxelotor (orange) compared to the curve prior to incubation (blue). Data shown as a mean (solid line) and standard deviation (shaded). (E) There was a significant decrease in the experimentally determined P₅₀ after samples were incubated with Voxelotor. ($\sigma_{\text{Untreated}}=32.6\text{mmHg}$, $\sigma_{\text{Treated}}=22.18\text{mmHg}$). Statistics were performed using a one-tailed, Wilcoxon signed rank test, $\alpha = 0.05$, * $p<0.05$, ** $p<0.01$).

Figure 4

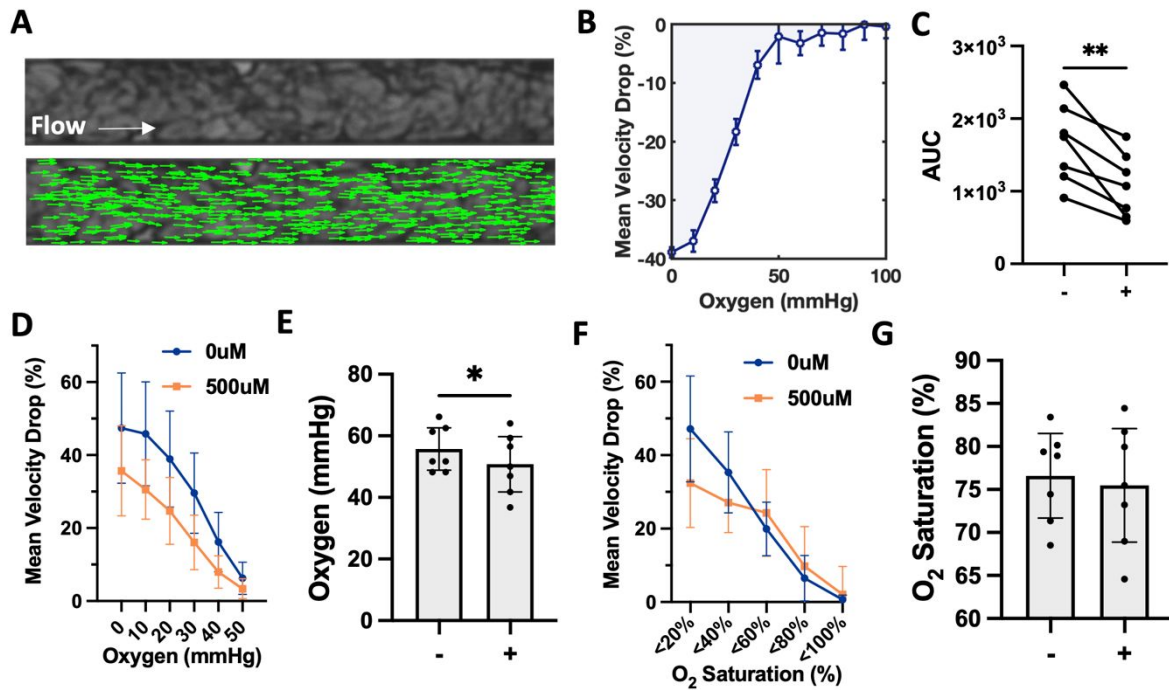


Figure 4 Increased Viscosity of SCD Blood During Hypoxia is Dependent on Hb-O₂ Saturation. (A) Representative image of blood flowing through the microfluidic channel (top). Green arrows represent the magnitude and direction of the recorded velocities of tracked features of interest (bottom). (B) Representative data from a single experiment showing the average percentage change in the mean velocity during each step of the oxygen cycling protocol. (Shown as mean \pm s.d.) The shaded region represents the area used to determine the area under the velocity response curve (AUC). (C) Pairwise comparison of AUC showing a significant reduction in oxygen-dependence when samples were incubated with Voxelotor. (D) Under severe hypoxia, treatment with Voxelotor decreased the mean velocity drop of sickle cell blood samples at specific pO₂ levels. Shown as mean with 95% CI. (E) The 3% velocity response threshold occurred at a slightly lower pO₂ after incubation with Voxelotor. (F) The mean velocity drop at specific levels of Hb-O₂ saturation was similar before and after incubation with Voxelotor. (G) 3% velocity response threshold before and after treatment shown using the measured values for Hb-O₂ saturation. Statistics were performed using a one- (C) or two-tailed (E and G), Wilcoxon signed rank test, $\alpha = 0.05$, * $p < 0.05$, ** $p < 0.01$).

Figure 5

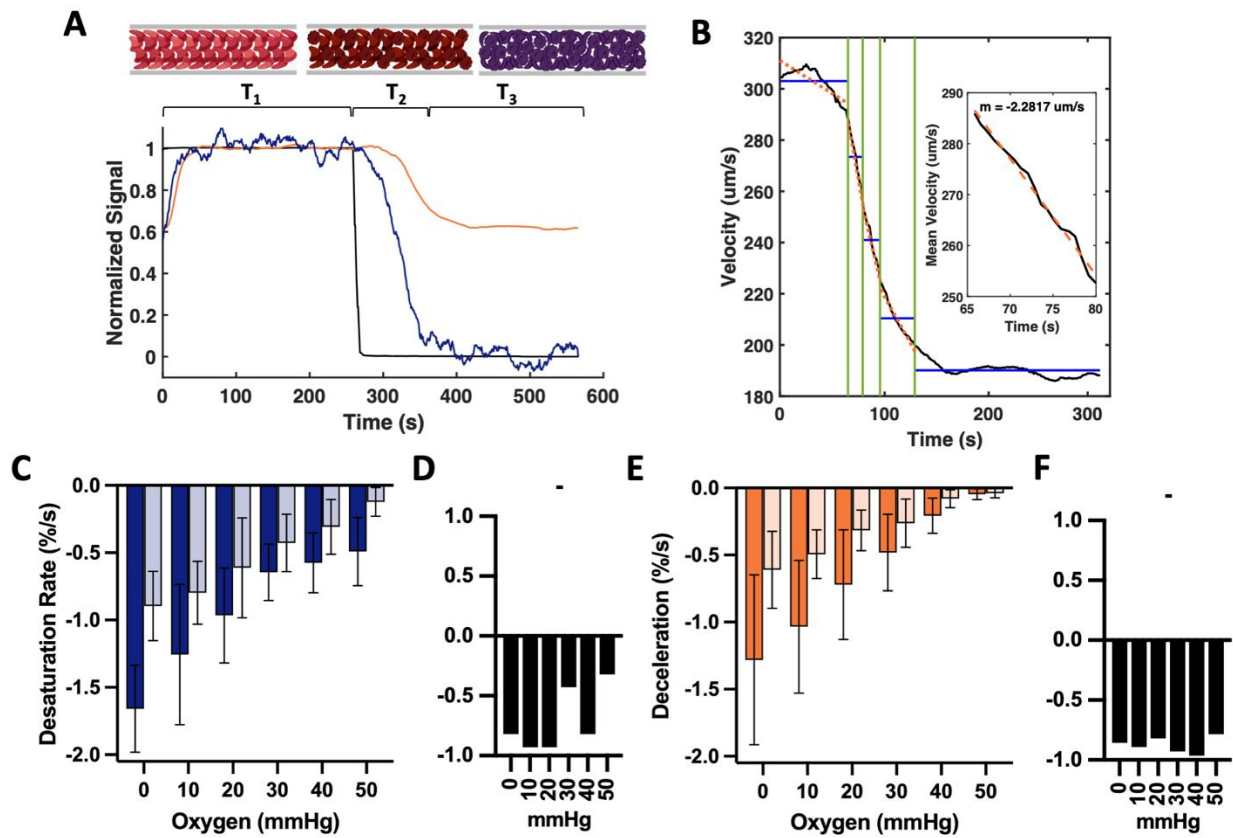


Figure 5 Transient Effects of Voxelator on Pathological Blood Flow (A) Tracked oxygen saturation (blue) and normalized mean velocity (orange) during transition to hypoxia. Schematics created with Biorender.com. (B) The transition region during the oxygen cycling protocol was analyzed using the `changepts()` function in Matlab. Four change points were identified where the mean signal change was largest. The data in each of these segments was fitted to a first-order polynomial to determine its slope (inset). (C) Desaturation rate during hypoxia of treated (light) and untreated (dark) samples. (D) Spearman correlation coefficient between p50 and desaturation prior to incubation with Voxelator. (E) Deceleration rate during hypoxia of treated (light) and untreated (dark) samples. (F) Spearman correlation coefficient between p50 and deceleration rate of untreated. Statistics were performed using a one-tailed, Wilcoxon signed rank test, $\alpha = 0.05$, * $p < 0.05$, ** $p < 0.01$ for panels C and E.